Int. J. Heat Mass Transfer. Vol. 27, No. 11, pp. 1999–2014, 1984.
Printed in Great Britain

0017-9310/84 $3.00 + 0.00
Pergamon Press Ltd.

Mechanistic modeling of pool entrainment phenomenon

ISAO KATAOKA
Institute of Atomic Energy, Kyoto University, Uji, Kyoto 611, Japan

and

MAMORU ISHII†
Reactor Analysis and Safety Division, Argonne National Laboratory, 9700 South Cass Avenue, Argonne, IL 60439, U.S.A.

(*Received* 5 *July* 1983 *and in revised form* 5 *January* 1984)

Abstract—Entrainment from a liquid pool with boiling or bubbling is of considerable practical importance in the safety evaluation of a nuclear reactor under off-normal transients or accidents such as loss-of-coolant and loss-of-flow accidents. Droplets which are suspended from a free surface are partly carried away by a streaming gas and partly returned back to the free surface by gravity. A correlation is developed for the pool entrainment amount based on simple mechanistic modeling and a number of data. This analysis reveals that there exist three regions of entrainment in the axial direction from a pool surface. In the first region (near surface region), entrainment is independent of height and gas velocity. In the second region (momentum controlled region), the amount of entrainment decreases with increasing height from the free surface and increases with increasing gas velocity. In the third region (deposition controlled region), the entrainment increases with increasing gas velocity and decreases with increasing height due to deposition of droplets. The present correlation agrees well with a large number of experimental data over a wide range of pressure for air–water and steam–water systems.

1. INTRODUCTION

ENTRAINMENT of liquid by gas flow is often encountered in various areas of engineering applications associated with heat and mass transfer. For example, in safety evaluations of nuclear reactors, entrainment can play an important role on analyzing heat and mass transfer processes under both off-normal operational and accident conditions. There are several different entrainment mechanisms depending on two-phase flow regimes [1, 2]. For annular dispersed flow, an onset of entrainment criterion [1], a correlation for the amount of entrained droplets [3], a correlation for droplet size and its distribution [4], and a correlation for entrainment rate [5] have been recently developed based on the shearing-off mechanism of roll-wave crests by a highly turbulent gas flow [1, 6]. Coupled with a theoretical formulation of two-fluid model [7], these correlations provide accurate predictions of thermo-hydraulics of annular dispersed flow.

Besides the above-mentioned phenomena, there is another important mechanism of entrainment. That is, the entrainment from a liquid pool by gas flow in boiling or bubbling. Earlier, in the field of nuclear engineering, this pool entrainment was studied in relation to radioactive carryover in a boiling water reactor [8], decontamination factors in evaporation of radioactive liquid waste in a natural circulation evaporator [9, 10], and steam generator performance. In the first two cases, entrainment has detrimental effects on reduction of radioactivity.

Recently the importance of the pool entrainment has been recognized associated with heat and mass transfer processes during loss-of-coolant accidents (LOCA), in particular, during the recovery phase of these accidents through reflooding of a core. In this case, pool entrainment may improve heat transfer, since droplets act as a heat sink through droplet evaporation. This will lead to lower vapor superheat and improved cooling of fuel pins which is quite important in terms of safety. Therefore, some research has been carried out on pool entrainment during LOCA [11] and reflooding [12, 13]. However, there have been no satisfactory correlations which predict the amount of entrainment at a given heat flux (or vapor velocity) and a given distance from the free liquid surface.

In the field of chemical engineering, pool entrainment has been studied in relation to the efficiency of the gas liquid contacting equipment, e.g. plate columns, etc. [14], and fluidized beds [15]. Some correlations have been recommended in this field [16]. However, geometry and operational conditions of this chemical engineering equipment are quite different from those of boilers and nuclear reactor systems. Therefore, these correlations may not be directly applied to later cases.

As for the pool entrainment in boilers, some experimental works have been carried out and several empirical correlations have been proposed [17–31]. However, these correlations are not based on physical modeling, therefore their applicability may be limited.

† To whom all correspondence should be addressed.

NOMENCLATURE

A_d	projected area of droplet
C_D	drag coefficient of droplet
C	coefficient in equation (36)
C_E	droplet concentration in gas space [kg m^{-3}]
C_K	coefficient in equation (2)
C_m	coefficient in equation (48)
$\dot{d}$	deposition rate of droplets [kg m^{-2} s^{-1}]
D	droplet diameter
D^*	dimensionless droplet diameter, $D/\sqrt{(\sigma/(g\Delta\rho))}$
D_B	bubble diameter
D_c	critical droplet diameter whose terminal velocity is equal to gas velocity
D_c^*	dimensionless critical droplet diameter, $D_c/\sqrt{(\sigma/(g\Delta\rho))}$
D_H	hydraulic diameter of vessel
D_H^*	dimensionless hydraulic diameter of vessel, $D_H/\sqrt{(\sigma/(g\Delta\rho))}$
D_{max}	maximum droplet diameter
D_{max}^*	dimensionless maximum droplet diameter, $D_{max}/\sqrt{(\sigma/(g\Delta\rho))}$
E_{fg}	entrainment defined by equation (1)
$E_{fg}(h, j_g)$	entrainment at height h and gas velocity j_g
$E_0(D, j_g)$	entrainment at interface which consists of droplets whose diameter are less than D (given by equation (13))
$f(D, j_g)$	droplet size distribution function for j_g
f_D	frequency of entrained droplet (in equation (14))
f_i	interfacial friction factor between gas and liquid ligament
F_D	drag force acting on droplet
g	acceleration due to gravity
$g(v_i, D, j_g)$	initial velocity distribution function for diameter D and gas velocity j_g
h	height above the pool surface
h^*	dimensionless height above the pool surface; $h/\sqrt{(\sigma/(g\Delta\rho))}$
h_1^*	dimensionless height defined by equation (50)
h_2^*	dimensionless height defined by equation (49)
h_m	maximum height of rising droplet
j_{fe}	superficial velocity of liquid flowing upward as droplet
j_f	total liquid volumetric flux
j_{fd}	droplet volumetric flux (superficial velocity) of falling drops
j_g	superficial gas velocity
j_g^*	dimensionless superficial gas velocity, $j_g/(\sigma g\Delta\rho/\rho_g^2)^{1/4}$
k_d	deposition coefficient of droplet [m s^{-1}]
l	length of liquid ligament
n_4	exponent in equation (48)
N	site density of entrained droplet (in equation (14))
$N_{\mu g}$	gas viscosity number, $\mu_g/(\rho_g\sigma\sqrt{[\sigma/(g\Delta\rho)]})^{1/2}$
$N_{\mu f}$	liquid viscosity number, $\mu_f/(\rho_f\sigma\sqrt{[\sigma/(g\Delta\rho)]})^{1/2}$
p	escape probability of entrained droplet (in equation (14))
P	system pressure
P_0	pressure around the bubble
Re_D	droplet Reynolds number, $\rho_g V_r D/\mu_g$
Re_g	gas Reynolds number, $\rho_g j_g D_H/\mu_g$
t	time
t_B	bubble burst time
v	velocity
v_f	velocity of element of liquid ligament
v_g	gas velocity
v_g^*	dimensionless gas velocity, $v_g/(\sigma g\Delta\rho/\rho_g^2)^{1/4}$
$v_h(D, j_g, h)$	initial velocity of droplet (diameter D) necessary to rise more than height h under gas velocity j_g
v_h^*	dimensionless form of v_h, $v_h/(\sigma g\Delta\rho/\rho_g^2)^{1/4}$
v_i	initial velocity of droplet at pool surface
v_i^*	dimensionless initial velocity, $v_i/(\sigma g\Delta\rho/\rho_g^2)^{1/4}$
$\bar{v}_i^*$	dimensionless initial velocity defined by equation (36)
v_r	relative velocity between droplet and gas
We_{max}	Weber number based on maximum droplet diameter defined by equation (44)
y	vertical position above pool surface
z	vertical coordinate attached to the liquid ligament.

Greek symbols

α	void fraction in liquid pool
$\delta(x)$	delta function defined by equation (38)
$\Delta\rho$	density difference between gas and liquid
$\dot{e}(j_g)$	entrainment rate at pool surface for j_g[kg m^{-2} s^{-1}]
μ_f	viscosity of liquid
μ_g	viscosity of gas
ρ_f	density of liquid
ρ_g	density of gas
σ	surface tension
τ_i	interfacial shear stress between gas and liquid ligament.

In view of these, a correlation for the pool entrainment is developed here from a simple physical model by considering droplet size distribution, initial velocity of entrained droplets, droplet motion and droplet deposition. It is shown to correlate a number of data over a wide range of experimental conditions.

2. PREVIOUS WORKS

In boiling or bubbling pool systems, droplets are entrained by the mechanisms of bubble bursting, splashing and foaming near the top of a pool. Some part of these entrained droplets fall back to the surface of a pool and the other part is carried away by streaming gas. The entrainment E_{fg} which is the ratio of the droplet upward mass flux $\rho_f j_{fe}$ to the gas mass flux $\rho_g j_g$, has been measured experimentally by some researchers [18–31]. Here j_{fe} is the superficial velocity of liquid flowing as droplets, and j_g is the superficial velocity of gas. Thus the entrainment E_{fg} is defined as

$$E_{fg} \equiv \frac{\rho_f j_{fe}}{\rho_g j_g}. \tag{1}$$

The experimental data show that the entrainment E_{fg} is a strong function of the gas superficial velocity j_g and the distance from the surface of a pool h. When the entrainment is plotted against the gas superficial velocity at a fixed distance h, at least three entrainment regimes can be observed [17, 20, 31]. In a low gas flux regime, the entrainment is small and entrained liquid consists of very fine droplets. In this regime, E_{fg} is approximately proportional to the gas flux. In an intermediate gas flux regime, larger drops are ejected from a pool and E_{fg} increases with j_g^{3-4}. At a higher gas flux, large gas slugs are formed and a pool is highly agitated. Then a considerable amount of liquid can be entrained by splashing. In this high gas flux regime, E_{fg} increases very rapidly with the gas flux, i.e. $E_{fg} \propto j_g^{7-20}$.

As for the effect of the distance from the surface of a pool, there are at least two distinct regions. In the first region (momentum controlled region), entrainment consists of larger droplets which rise due to their initial momentum at the surface and smaller droplets which are carried away by streaming gas. In this region, E_{fg} decreases rapidly with increasing distance, i.e. $E_{fg} \propto h^{-3}$. In the second region (deposition controlled region), entrainment consists only of small droplets whose terminal velocity is smaller than the gas velocity. Entrainment in this region decreases gradually due to the droplet depositions. This trend can be expressed as an exponential decay function of the height.

Although there have been no theoretical methods of predicting entrainment, several semi-empirical correlations [19, 22, 28] based on various data [18, 20, 21, 23, 26, 31] and dimensional analyses have been proposed.

Kruzhilin [19] proposed a dimensionless correlation for the intermediate gas flux regime and momentum controlled region based on a dimensional analysis. With an assumption that the initial velocity of droplets at the interface is determined by the kinetic energy of vapor $\rho_g j_g^2/2$, he obtained

$$E_{fg} = C_K j_g^{*4} \sqrt{\left(\frac{\Delta\rho}{\rho_g}\right)} \sqrt{\left(\frac{\Delta\rho}{\rho_f}\right)}. \tag{2}$$

Here j_g^* is the dimensionless gas flux (see nomenclature). In equation (2), C_K must be determined from experimental data. However, it has been found that the value of C_K depends on the distance from the interface. Although equation (2) shows the effects of velocity and pressure on E_{fg}, it does not give any information on the effect of height, which is important in the momentum controlled region.

Sterman [22] correlated the experimental data of entrainment for steam–water systems at pressures from 0.1 to 18 MPa, and proposed a dimensionless correlation. His correlation depends on the average void fraction in the pool, therefore, he has also proposed several void fraction correlations applicable to the problem. For a reasonably large vessel satisfying the condition given by

$$D_H^* \left(\frac{\Delta\rho}{\rho_g}\right)^{0.2} > 260 \tag{3}$$

where D_H^* is the dimensionless diameter of vessel, the Sterman correlation can be simplified to

$$E_{fg} = 6.09 \times 10^9 j_g^{*2.76} h^{*-2.3} \left(\frac{\rho_g}{\Delta\rho}\right)^{-0.26} N_{\mu f}^{2.2} \left(\frac{\Delta\rho}{\rho_f}\right)^{1.1}. \tag{4}$$

Here h^* is the dimensionless height, and $N_{\mu f}$ is the liquid viscosity number based on liquid viscosity μ_f (see nomenclature).

Equation (4) is applicable to the intermediate gas flux regime and momentum controlled region. The boundary between the intermediate and high gas flux regimes occurs at

$$j_g^* = 1.08 \times 10^{-5} h^{*0.83} \left(\frac{\Delta\rho}{\rho_g}\right)^{-0.2} N_{\mu f}^{-0.92} \left(\frac{\rho_f}{\Delta\rho}\right)^{0.46}. \tag{5}$$

The Sterman correlation shows a strong dependence of E_{fg} on the liquid viscosity through the liquid viscosity number $N_{\mu f}$. According to this correlation, entrainment increases with the liquid viscosity as $E \propto \mu_f^{2.2}$. However, experimental data on the effect of the liquid viscosity on entrainment [24] does not show such a strong viscosity dependence. Furthermore, equation (4) fails to predict experimental data of air–water systems [23].

Rozen *et al.* [28] proposed a correlation for the deposition controlled region, in terms of the critical droplet size. Therefore, for this correlation the size of droplet should be specified. By matching the settling velocity of wake regime droplets to the gas flux, this drop size may be specified [5, 32]. By using this

approach, the Rozen correlation can be given by

$$E_{fg} = 7.6\times10^{-5}\{j_g^{*}N_{\mu g}^{1/6}+4870j_g^{*4.2}N_{\mu g}^{0.7}\} \times\sqrt{\left(\frac{\Delta\rho}{\rho_g}\right)}e^{-0.23h/D_H} \quad (6)$$

where $N_{\mu g}$ is the gas velocity number based on gas viscosity μ_g. The correlation given by equation (6) shows basically two regimes depending on the value of j_g^*. For small j_g^*, equation (6) can be approximated as

$$E_{fg} = 7.6\times10^{-5}j_g^{*}N_{\mu g}^{1/6}\sqrt{\left(\frac{\Delta\rho}{\rho_g}\right)}e^{-0.23h/D_H}. \quad (7)$$

On the other hand, for large j_g^* equation (6) can be simplified to

$$E_{fg} = 0.37j_g^{*4.2}N_{\mu g}^{0.7}\sqrt{\left(\frac{\Delta\rho}{\rho_g}\right)}e^{-0.23h/D_H}. \quad (8)$$

The transition occurs at

$$j_g^{*} = 0.071N_{\mu g}^{1/6}. \quad (9)$$

As shown above, these semi-empirical correlations based on dimensional analyses are applicable to limited ranges of operational parameters. Furthermore, some parametric dependencies predicted by these correlations may not be correct if they are applied beyond the ranges of the data base. In view of the importance of entrainment from a liquid pool in various engineering problems as well as safety analyses of nuclear reactors, an accurate correlation applicable over wide ranges of operational parameters is highly desirable. For this general purpose, the correlation should be based on realistic modeling of droplet behaviors in the vapor space and at the liquid vapor interface.

Based on these observations, a correlation for pool entrainment is developed from mechanistic modeling in this study. It takes into account the droplet diameter distribution, initial velocity of droplets and droplet motion. Thus the present model reflects more realistic mechanisms of pool entrainment than those proposed previously.

3. BASIC EQUATION

When boiling or bubbling occurs in a liquid pool, droplets are ejected from a pool surface by bursting of bubbles, splashing or foaming. These droplets have varying diameters and ejection velocities. Each droplet goes through its own trajectory depending on its mass, initial velocity, and drag force exerted by streaming gas. The entrained droplet flux is determined by the collective behavior of each droplet, which can be analyzed by solving an equation of motion of each droplet using the initial condition at the interface. However, there are an enormous number of droplets ejected from the surface of a liquid pool, thus it is impractical to treat the movement of each droplet separately. Therefore, a statistical treatment has been adopted here.

In order to treat the entrainment problem statistically, one needs to introduce important physical parameters and distribution functions at the interface such as the entrainment rate at the interface, droplet size distribution function, droplet initial velocity distribution, and necessary initial velocity of a droplet to rise more than height, h. The entrainment rate at the interface, $\dot{e}(j_g)$, is the mass flux of droplets at the interface and is considered to be a function of the gas velocity. Droplets ejected from the interface have various diameters represented by the droplet size distribution function $f(D, j_g)$, which is the fraction of droplets whose diameter lies between D and $D+dD$. This function is considered to depend on the gas velocity. Furthermore, $f(D, j_g)$ satisfies the following relation

$$\int_0^\infty f(D,j_g)\,dD = 1. \quad (10)$$

The initial velocity v_i, which is the velocity of the droplet just ejected from the interface, has its own distribution function, $g(v_i, D, j_g)$. This function represents the fraction of droplets whose velocity lies between v_i and v_i+dv_i at the interface. It also satisfies

$$\int_0^\infty g(v_i, D, j_g)\,dv_i = 1. \quad (11)$$

In view of the mechanisms of droplet ejection, this function is considered to depend on the droplet diameter and gas velocity.

The velocity of a droplet necessary to rise more than h, $v_h(D, j_g, h)$ can be obtained by solving the equation of motion of a single droplet with an appropriate drag coefficient. Thus it should be a function of the droplet diameter, gas velocity and height from the interface.

Using the above-mentioned statistical parameters, the entrainment at distance h from the interface can be given by the following integral

$$E_{fg}(h,j_g) = \frac{\dot{e}(j_g)}{\rho_g j_g}\int_0^\infty\int_{v_h(D,j_g,h)}^\infty g(v_i, D, j_g)f(D,j_g)\,dv_i\,dD. \quad (12)$$

The entrainment given by equation (12) consists of two groups of droplets. The first group of droplets are the ones whose diameters are larger than the critical droplet diameter D_c. Here D_c is the diameter of a droplet whose terminal velocity is equal to the gas velocity. Therefore, this group of droplets arrive at the height by the initial momentum gained at ejection. The second group of droplets have their diameters less than the critical droplet diameter D_c. This group of droplets can be carried away by the streaming gas to any height unless they are deposited to the wall.

4. DROPLET DIAMETER DISTRIBUTION AND ENTRAINMENT RATE AT INTERFACE

The droplet diameter distribution function $f(D, j_g)$ and entrainment rate at interface $\dot{e}(j_g)$ are key factors to determine entrainment at any height from the pool

surface. However, these two parameters are difficult quantities to analyze or measure directly. Thus one needs to consider a more directly observable parameter. For this purpose the interface entrainment $E_0(D, j_g)$ is introduced. $E_0(D, j_g)$ represents the entrainment consisting of droplets whose diameters are less than the stated value D. Then it can be expressed as

$$E_0(D,j_g) = \frac{\dot{e}(j_g)}{\rho_g j_g} \int_0^D f(D,j_g)\,dD. \tag{13}$$

It is noted that Garner *et al.* [18] have measured $E_0(D, j_g)$.

Now, instead of using a completely empirical correlation, a simple model for $E_0(D, j_g)$ is developed by considering the mechanisms of entrainment. By introducing the droplet site density N, mean frequency f_D, escape probability p and drag force F_D, the parameter $E_0(D, j_g)$ may be related to these by

$$E_0(D,j_g) \sim N f_D p F_D. \tag{14}$$

The drag force F_D[32] is given by

$$F_D = -\tfrac{1}{2} C_D \rho_g v_r |v_r| A_d \tag{15}$$

where C_D, v_r, and A_d are the drag coefficient, relative velocity, and projected area of a droplet, respectively. For a wake regime (Re_D = 5–1000), the drag coefficient C_D[5, 32] is approximately given by

$$C_D = \frac{10.67}{Re_D^{0.5}}. \tag{16}$$

Here Re_D is the droplet Reynolds number for a dilute suspension (see nomenclature). For a simple model, the following approximations may be used.

$$v_r|v_r| \sim j_g^2$$
$$A_d \sim D^2. \tag{17}$$

Substituting equations (15)–(17) into equation (14) one obtains

$$E_0(D,j_g) \sim (j_g D)^{1.5}. \tag{18}$$

The experimental data of Garner *et al.* [18] for $E_0(D, j_g)$ are plotted against $D^* j_g^*$ in Fig. 1. Here j_g^* is the nondimensional gas flux and D^* is the nondimensional drop diameter (see nomenclature). As predicted by equation (18), experimental data for $D \leqslant D_c$ can be well correlated by

$$E_{fg}(h,j_g,D) = 0.3975(D^* j_g^*)^{1.5}. \tag{19}$$

However, it should be noted that the correlation given by equation (19) is based on a data set taken at one pressure. As equation (14) indicates, there should be an additional pressure effect through the density ratio $\Delta\rho/\rho_g$ in equation (19). This becomes clear in the latter analyses and the exponent of $\Delta\rho/\rho_g$ is determined to be -1 in comparison with experimental data (see Section 8) [33]. This empirical result is used from this stage in order to simplify the subsequent analysis. The detailed development is given elsewhere [33].

Then equation (19) can be modified and in view of

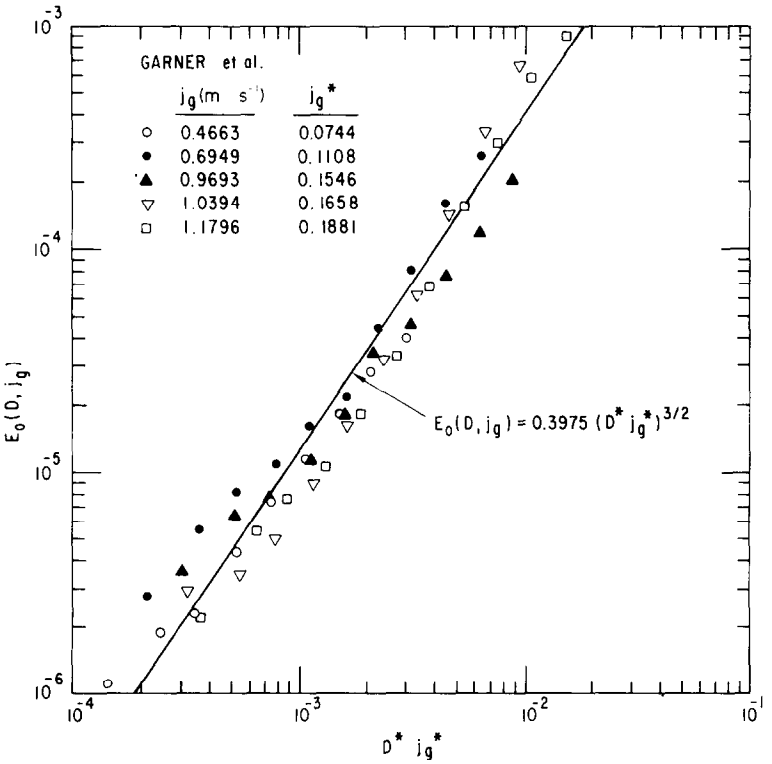

FIG. 1. Entrainment below stated value $E_0(j_g, D)$ vs dimensionless diameter $D^* j_g^*$ for the data of Garner *et al.* [18].

equation (13)

$$\frac{\dot{\varepsilon}(j_g)}{\rho_g j_g}\int_0^D f(D,j_g)\,dD \equiv E_0(D,j_g)$$

$$= 2.48\times 10^{-4}\left(\frac{\rho_g}{\Delta\rho}\right)^{-1.0}(D^* j_g^*)^{1.5}. \quad (20)$$

By differentiating equation (20) with respect to D

$$\sqrt{\left(\frac{\sigma}{g\Delta\rho}\right)}\frac{\dot{\varepsilon}(j_g)}{\rho_g j_g}f(D,j_g) = 3.72\times 10^{-4}$$

$$\times\left(\frac{\rho_g}{\Delta\rho}\right)^{-1.0} j_g^{*1.5} D^{*0.5}. \quad (21)$$

This is an important correlation relating the entrainment rate and droplet diameter distribution function to the gas flux and droplet diameter.

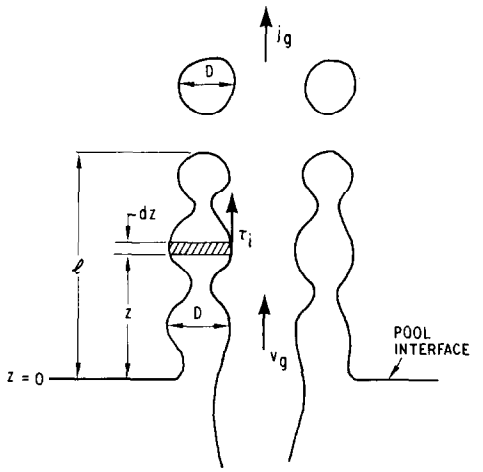

FIG. 2. Schematic diagram of droplet entrainment.

5. DROPLET VELOCITY AT INTERFACE

When the gas flux j_g is small, the flow regime in a pool is a bubbly flow. In this regime, discrete bubbles rise up to the surface of the pool and collapse there. This mechanism of the bubble burst and subsequent entrainment have been studied previously and expressions for the velocity of entrained droplets has been developed empirically and theoretically [34–38]. According to Newitt *et al.* [35], the initial velocity of an entrained droplet due to bubble burst is given by

$$v_i = \frac{3}{2}\frac{t_B}{D_B\rho_f}\left(\frac{4\sigma}{D_B}+P_0\right) \quad (22)$$

where t_B, D_B, and P_0 are bubble burst time, bubble diameter, and pressure around the bubble.

However, for pool entrainment, the bubbly flow regime is limited to a very small gas velocity. For example, in an air–water system at atmospheric pressure, the flow regime transition from bubbly to churn turbulent flow occurs at j_g in the order of 10 cm s^{-1} [39]. Applying the drift flux model [40] to a bubbling system and using the transition criterion from bubble to churn turbulent flow regime [41] given by $\alpha \simeq 0.3$, the transition gas flux becomes

$$j_g^* = 0.325\left(\frac{\rho_g}{\rho_f}\right)^{1/2}. \quad (23)$$

This indicates that the churn turbulent flow may be the most dominant flow regime in a bubbling pool. In the case of churn turbulent flow, the initial velocity of entrained droplets is not determined by the bubble burst mechanism, but by a momentum exchange mechanism suggested by Nielsen *et al.* [42].

This momentum exchange mechanism is shown schematically in Fig. 2. It is assumed that droplets are generated by shearing-off of film like liquid ligaments and the shear stress due to streaming gas has a dominant effect on this shearing process. The equation of motion for an element of the liquid ligament is given by

$$\rho_f D\frac{dv_f}{dt} = \tau_i - \Delta\rho g D \quad (24)$$

where v_f is the velocity of an element of a liquid ligament at z. And the interfacial shear stress τ_i is given in terms of interfacial friction factor f_i as

$$\tau_i = f_i\tfrac{1}{2}\rho_g v_g^2. \quad (25)$$

When the gravity term is negligible compared with the interfacial term, equation (24) can be rewritten as

$$\frac{dv_f}{(1/2)(\rho_g/\rho_f)(1/D)f_i v_g^2} = dt = \frac{dz}{v_f}. \quad (26)$$

At $z = l$, this velocity is equal to the initial velocity of the droplet, that is

$$v_f(z = l) = v_i. \quad (27)$$

Integrating equation (26) from $z = 0$ to l, one can obtain

$$\tfrac{1}{2}\rho_f v_i^2 D = \tfrac{1}{2}f_i\rho_g v_g^2 l. \quad (28)$$

Equation (28) implies that the kinetic energy of the droplet entrained is equal to the work exerted on the element of a liquid ligament by gas flow.

The ligament of liquid at the pool interface, as shown in Fig. 2, can be regarded as a sequence of several droplets which are about to be entrained. Therefore, the interfacial shear stress may be related to the drag coefficient for a droplet in the wake regime, i.e. equation (16), thus

$$f_i \sim C_D \sim Re_D^{-0.5}. \quad (29)$$

The length of the liquid ligament is assumed to be proportional to the width of the ligament which is of the order of the droplet diameter in analogy with the Rayleigh instability of a liquid jet. Then

$$l \sim D. \quad (30)$$

Substituting equations (29) and (30) into equation (28),

one obtains

$$v_i^* \sim v_g^{*3/4} N_{\mu g}^{1/4} D^{*-1/4} \left(\frac{\rho_g}{\rho_f}\right)^{1/2} \tag{31}$$

where v_i^* and v_g^* are the dimensionless initial velocity and gas velocity.

The gas velocity v_g is related to the superficial gas velocity j_g in terms of void fraction α in the liquid pool as

$$v_g = \frac{j_g}{\alpha}. \tag{32}$$

Then equation (31) can be rewritten as

$$v_i^* \sim j_g^{*3/4} \alpha^{-3/4} N_{\mu g}^{1/4} D^{*-1/4} \left(\frac{\rho_g}{\rho_f}\right)^{1/2}. \tag{33}$$

Equation (33) is derived from the consideration of the momentum exchange mechanism at the interface. However, there are some experimental data for v_i, which support the dependence of v_i on j_g and D as given by equation (33).

Akselrod and Yusova [43] and Cheng and Teller [14] measured indirectly (calculated from the maximum height of a droplet) the droplet initial velocity in an air–water system at atmospheric pressure. In their experiments, the liquid level is very low, i.e. 5–6 mm for Akselrod and Yusova [43] and 38 mm for Cheng and Teller [14]. Under these conditions, a steady gas jet should form at the pool interface as observed by Muller and Prince [44]. For this case α is almost independent of j_g. Therefore, in Fig. 3, the experimental data of Akselrod and Yusova [43] and Cheng and Teller [14] are plotted in the $v_i^*/\{j_g^{*3/4} N_{\mu g}^{1/4} \times (\rho_g/\rho_f)^{1/2}\}$ vs D^* plane. It can be seen that the experimental data for the initial velocity of droplets are well correlated by

$$v_i^* = 205 j_g^{*3/4} N_{\mu g}^{1/4} D^{*-1/4} \left(\frac{\rho_g}{\rho_f}\right)^{1/2}. \tag{34}$$

There are no data which can be used to determine the dependence of v_i on α directly. It is expected, however, that v_i depends on α as predicted by the present model given by equation (33).

For a system with a much higher liquid level, which is of considerable practical importance, the void fraction is a function of the gas superficial velocity j_g. For this case a correlation between α and j_g is necessary. The void fraction in a liquid pool generally shows lower values than those predicted by the one-dimensional drift-flux model. This is mainly due to the recirculation of liquid in the pool. Some empirical correlations for the void fraction are available for this kind of flow [45–48].

These void fraction correlations have been reviewed in detail [17, 33], and it appears that the following relation is most appropriate for pool entrainment [33]

$$\alpha \sim j_g^{*2/3} D_H^{*-0.28} \left(\frac{\rho_g}{\Delta\rho}\right)^{-0.153}. \tag{35}$$

Substituting equation (35) into equation (33), one obtains

$$v_i^* = C j_g^{*1/4} N_{\mu g}^{1/4} D^{*-1/4} \left(\frac{\rho_g}{\rho_f}\right)^{1/2} \times D_H^{*-0.21} \left(\frac{\rho_g}{\Delta\rho}\right)^{-0.11} \equiv \bar{v}_i^*. \tag{36}$$

Here C is a proportionality constant which should be determined in collaboration with experimental data.

It is noted here that actually the initial velocity of a droplet at the pool interface should have its distribution as discussed in Section 3. However, apparently no data are available due to experimental difficulties. Therefore, as a first approximation, only the mean value of the initial velocities expressed by the above correlation is used in this analysis. This may also be justified for the simplicity of the model which can be checked by experimental data. Then the droplet velocity distribution function, $g(v_i, D, j_g)$ is given by the delta function in the following form

$$g(v_i, D, j_g)\, dv_i = \delta(v_i^* - \bar{v}_i^*)\, dv_i^* \tag{37}$$

where

$$\left.\begin{aligned} &\int_{-\infty}^{\infty} \delta(x)\, dx = 1 \\ &\delta(x) = 0 \quad \text{for} \quad x \neq 0. \end{aligned}\right\} \tag{38}$$

In other words, the initial velocity distribution over the same size droplets is neglected.

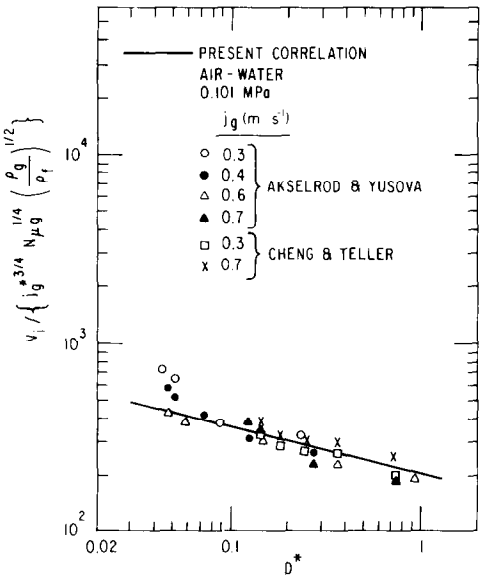

FIG. 3. Initial velocity of droplet in the $v_i^*/\{j_g^{*3/4} N_{\mu g}^{*1/4} (\rho_g/\rho_f)^{1/2}\}$ vs D^* plane for the data of Akselrod and Yusova [43] and Cheng and Teller [14].

6. MAXIMUM HEIGHT OF RISING DROPLET

The maximum height which can be attained by a rising droplet in gas flowing vertically upward can be calculated by solving the equation of motion of the droplet by specifying the drag coefficient [33, 49]. An analytical solution for a practical range of the droplet Reynolds number (Re_D = 5–1000) has been obtained [33]. From the maximum height of a rising droplet, the droplet velocity $v_h(D,j_g,h)$ necessary to rise more than a height h can be calculated as an inverse function.

The equation of motion of a droplet in a gas stream is formulated by

$$\frac{dv}{dt} = -\frac{\Delta\rho}{\rho_f}g - \frac{3}{4}C_D\frac{1}{D}\frac{\rho_g}{\rho_f}(v-v_g)|v-v_g| \quad (39)$$

with initial condition, $v = v_i$, $y = 0$ at $t = 0$. Here v, t, and y are the droplet velocity, time, and height from the pool surface.

In Fig. 4, the maximum height calculated based on equations (39) and (16) for $v_i/j_g = 1$, $v_i/j_g = 2$, and $v_i/j_g = 10$ is plotted against the diameter ratio D/D_c where D_c is the critical diameter having the terminal velocity equal to j_g. Here it is noted that in the region above the pool, the liquid fraction is small. Thus v_g is approximately j_g.

As mentioned above, the initial velocity of a droplet necessary to rise more than a height h is obtained as a function of D, j_g and h. It is a complicated function, therefore, the analytical solution is not presented here. However, calculations based on equations (39) and (16) indicate that the effect of j_g is not so strong for the practical range of j_g. From this observation, therefore, $v_h(D,j_g,h)$ may be approximated by the following simple expression for the range of j_g corresponding to bubbly or churn turbulent flow

$$\begin{aligned} v_h &= 0 && (D < D_c) \\ v_h &= \sqrt{\left(2gh\frac{\Delta\rho}{\rho_f}\right)} && (D \geqslant D_c). \end{aligned} \quad (40)$$

This equation can be obtained from a balance between the kinetic energy and potential energy by neglecting the work done by the drag force for $D \geqslant D_c$. As mentioned above this assumption can be justified as a first-order approximation where the magnitude of v_i/j_g is of the order of unity. Equation (40) can be rewritten in a dimensionless form as

$$\begin{aligned} v_h^* &= 0 && (D^* < D_c^*) \\ v_h^* &= \sqrt{(2h^*)}\left(\frac{\rho_g}{\rho_f}\right)^{1/2} && (D^* \geqslant D_c^*) \end{aligned} \quad (41)$$

where v_h^* and D_c^* are the dimensionless form of v_h and D_c (see nomenclature). For the wake regime D_c^* is given by

$$D_c^* = 4j_g^* N_{\mu g}^{1/3}. \quad (42)$$

7. CORRELATION FOR ENTRAINMENT AMOUNT

In previous sections, the entrainment rate and droplet size distribution at the pool interface, initial droplet velocity, and velocity necessary to rise more than a height h, are obtained. Now the amount of entrainment can be calculated using the basic expression for entrainment and these results. Hence by substituting equations (21), (37), and (41) into equation (12) one obtains

$$E_{fg}(h,j_g) = \int_0^\infty \int_{v_h^*}^\infty \delta(v_i^* - \bar{v}_i^*) \times 3.72 \times 10^{-4} \times \left(\frac{\rho_g}{\Delta\rho}\right)^{-1.0} j_g^{*1.5} D^{*0.5}\, dv_i^*\, dD^*. \quad (43)$$

Droplets have finite diameters, therefore, the range of the integration over D^* will be limited by the maximum diameter of droplets D_{max}. D_{max} is often correlated in terms of the maximum droplet Weber number [50, 4] defined by

$$We_{max} \equiv \frac{D_{max}\rho_g j_g^2}{\sigma} = D_{max}^* j_g^{*2} \quad (44)$$

where D_{max}^* is the dimensionless maximum droplet diameter. For example, for falling droplets [50] the maximum droplet diameter is given by

$$We_{max} = 22 \quad \text{or} \quad D_{max}^* = 22 j_g^{*-2}. \quad (45)$$

On the other hand, in annular-dispersed flow, the maximum droplet diameter is given by [4]

$$We_{max} = 0.031 Re_g^{2/3}\left(\frac{\rho_g}{\rho_f}\right)^{-1/3}\left(\frac{\mu_g}{\mu_f}\right)^{2/3} \quad (46)$$

where Re_g is the gas Reynolds number. Equation (46)

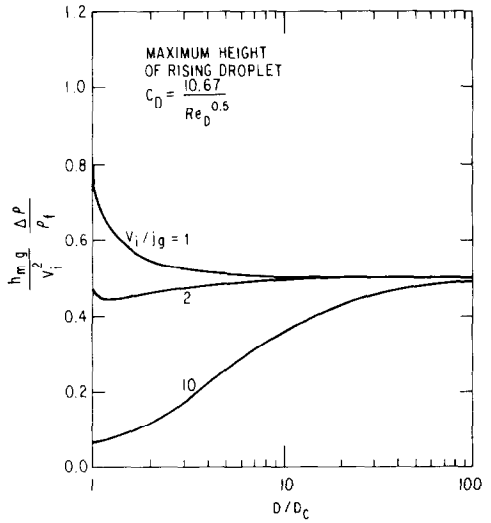

FIG. 4. Maximum height of rising droplet for wake regime.

shows that D^*_{max} can be scaled by

$$D^*_{max} \sim j^{*-4/3}_g. \quad (47)$$

In view of the entrainment mechanism discussed in previous sections, the maximum droplet diameter in pool entrainment is assumed to be given by a form similar to equations (45) and (47). Thus

$$D^*_{max} = C_m j^{*-n_4}_g \quad (48)$$

where C_m and n_4 should be determined in collaboration with experimental data in the absence of a detailed hydrodynamic model of the droplet generation.

Integrating equation (43) with equation (48), one obtains the following results.

For

$$h^* \leqslant \frac{C^2}{2}\frac{1}{\sqrt{C_m}} j^{*(n_4+1)/2}_g N^{1/2}_{\mu g} D^{*-0.42}_H \left(\frac{\rho_g}{\Delta\rho}\right)^{-0.23} \equiv h^*_2$$

$$E_{fg}(h, j_g) = 2.48 \times 10^{-4} C^{1.5}_m j^{*1.5-3n_4/2}_g \left(\frac{\rho_g}{\Delta\rho}\right)^{-1.0}. \quad (49)$$

For

$$h^* \geqslant \frac{C^2}{4} N^{1/3}_{\mu g} D^{*-0.42}_H \left(\frac{\rho_g}{\Delta\rho}\right)^{-0.23} \equiv h^*_1$$

$$E_{fg}(h, j_g) = 1.99 \times 10^{-3} j^{*-3}_g N^{1/2}_{\mu g} \left(\frac{\rho_g}{\Delta\rho}\right)^{-1.0}. \quad (50)$$

For

$$h^*_2 \leqslant h^* \leqslant h^*_1$$

$$E_{fg}(h, j_g) = 3.10 \times 10^{-5} C^6 j^{*3}_g h^{*-3} N^{1.5}_{\mu g} D^{*1.25}_H \left(\frac{\rho_g}{\Delta\rho}\right)^{-0.31}. \quad (51)$$

Equations (49)–(51) show that there are three regions in terms of the height from the pool interface. The first region (near surface region) is limited to small h. The entrainment and limit on height are given by equation (49). In this region, entrainment consists of all droplets which are entrained at the pool interface. The second region (momentum controlled region) is limited to intermediate h. In this region, entrainment consists of droplets which can attain height h due to the initial momentum of droplets. As the correlation given by equation (51) indicates, the entrainment amount increases with increasing gas velocity and with decreasing height in the second region. The third region (deposition controlled region) applies to large h. In this region, entrainment consists of droplets whose terminal velocity is less than the gas velocity. Equation (50) indicates that E_{fg} is independent of h. In the actual system, droplets can deposit on the vessel wall and thus E_{fg} should decrease gradually with increasing height.

In Fig. 5, the general trend of the entrainment E_{fg} is shown schematically. Indeed, the same trend is also observed in various experiments [25, 26]. Equations

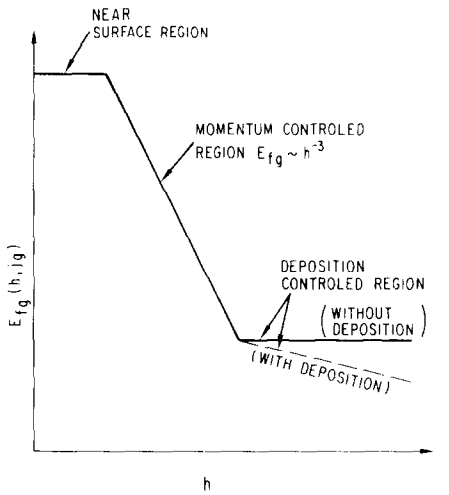

FIG. 5. General trend of effects of height, h, on entrainment E_{fg}.

(49)–(51) indicate significant dependence of the entrainment amount on the height above the pool surface and gas velocity. The behavior of entrainment characteristic significantly changes as a function of height as indicated by the existence of three regions. For practical applications the proportionality constants and effects of physical properties of liquid and gas reflected in exponent n_4 should be correlated in collaboration with experimental data.

8. ENTRAINMENT AMOUNT IN MOMENTUM CONTROLLED REGIME

Several experiments have been carried out to study entrainment amount in a bubbling or boiling pool. Most of the experimental data fall in the momentum controlled region which is most important in view of practical applications. It is also noted that in this region the entrainment is a very strong function of the height, whereas in the other two regimes the effect of height is not very important. In view of these, the entrainment in this region will be discussed first.

Among available data, those of Kolokoltsev [31] (steam–water, 0.129 MPa), Garner *et al.* [18] (steam–water, 0.101 MPa), Sterman and co-workers [21, 22] (steam–water, 1.72–18.7 MPa), Golub [26] (air–water, 0.101 MPa) and Styrikovich *et al.* [23] (air–water, 0.11–5.0 MPa) are used for the present correlation purpose because in these experiments the gas velocity and measurement location above the pool surface have been varied systematically. The key parameters of these experiments are summarized in Table 1.

In Figs. 6 and 7, some typical experimental data for the entrainment are plotted against a parameter j^*_g/h^*. However, Fig. 8 shows the data of Golub [26] in the E_{fg}/j^{*3}_g vs h^* plane. This is because in his experiments h^* has been varied extensively, and in this plot the dependence of E_{fg} on h^* can be easily examined. It is noted that his data also include the entrainment

Table 1. Summary of various experiments on entrainment amount from liquid pool

Reference	Fluid	Vessel diameter D_H(m)	Height above pool surface, h(m)	Pressure (MPa)	j_g(m s^{-1})
Kolokoltsev [31]	Steam–water	0.30	0.5 0.6	0.129	1.0–1.7
Garner *et al.* [18]	Steam–water	0.30	0.5–1.0	0.101	0.3–1.3
Sterman and co-workers [21, 22]	Steam–water	0.24	0.5–0.9	1.72–18.7	0.01–1.3
Styrikovich *et al.* [23]	Air–water	0.10	0.26–0.72	0.11–5.0	0.1–1.7
Golub [26]	Air–water	0.20	0.1–2.2	0.101	0.5–2.0
Rozen *et al.* [29]	Air–water	0.20	0–0.35	0.101	0.6–3.0

amount in the deposition controlled region. Figure 8 verifies the dependence of the entrainment on the height above the pool surface as predicted by equations (49)–(51) and indicated schematically in Fig. 5.

As shown in Figs. 6 and 7, the entrainment amount increases with the third power of j_g^*/h^*, which is also predicted by the present model by equation (51). In collaboration with these experimental data, the proportionality constant C in equation (51) is determined. Then the final form of the correlation for the entrainment in the momentum controlled region is given by

$$E_{fg}(h,j_g) = 5.42\times 10^6 j_g^{*3} h^{*-3} N_{\mu g}^{1.5} \times D_H^{*1.25}\left(\frac{\rho_g}{\Delta\rho}\right)^{-0.31}. \quad (52)$$

It should be noted that this equation corresponds to equation (4) given by Sterman [22]. However, equation (4) does not agree with air–water experimental data, whereas the present correlation agrees with both steam–water and air–water data. This is because the present correlation includes the effect of the gas viscosity through $N_{\mu g}$ which is important for the transport of droplets in the gas phase.

Figure 9 shows the comparison of various data to the above correlation in the $E_{fg}/\{N_{\mu g}^{1.5} D_H^{*1.25}(\rho_g/\Delta\rho)^{-0.31}\}$ vs j_g^*/h^* plane. As can be seen from this comparison, equation (52) satisfactorily correlates the wide range of experimental data for entrainment in the momentum controlled region. Further comparisons of data to the correlation are shown in Figs. 6 and 7. This correlation applies to the intermediate gas flux regime.

Figure 9 shows that at low values of j_g^*/h^*, the dependence of the entrainment on j_g^*/h^* changes. This

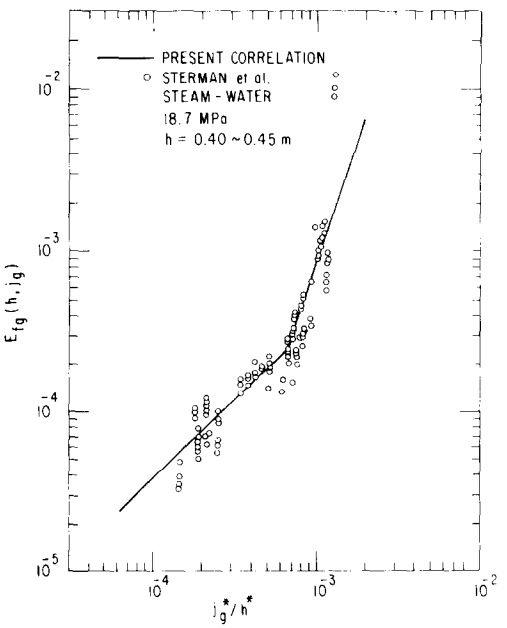

FIG. 6. Comparison of experimental data of Sterman and co-workers [21, 22] with predicted entrainment at 18.7 MPa.

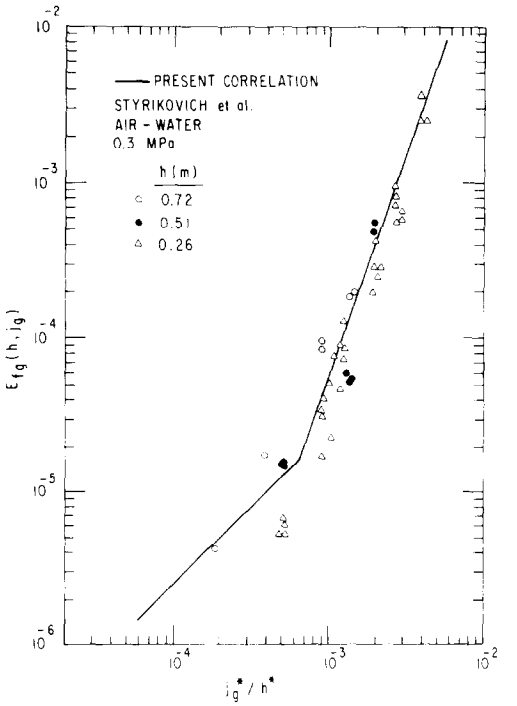

FIG. 7. Comparison of experimental data of Styrikovich *et al.* [23] with predicted entrainment at 0.3 MPa.

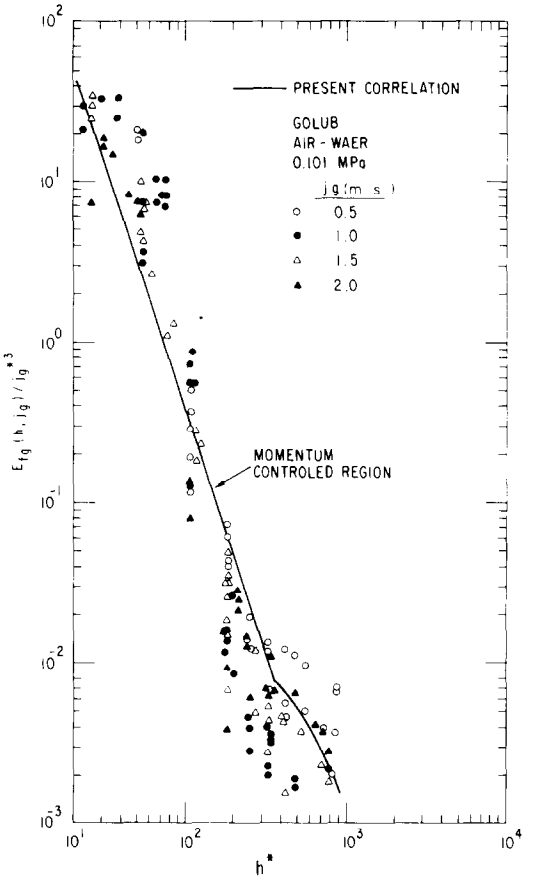

FIG. 8. Comparison of experimental data of Golub [26] with predicted entrainment at 0.101 MPa.

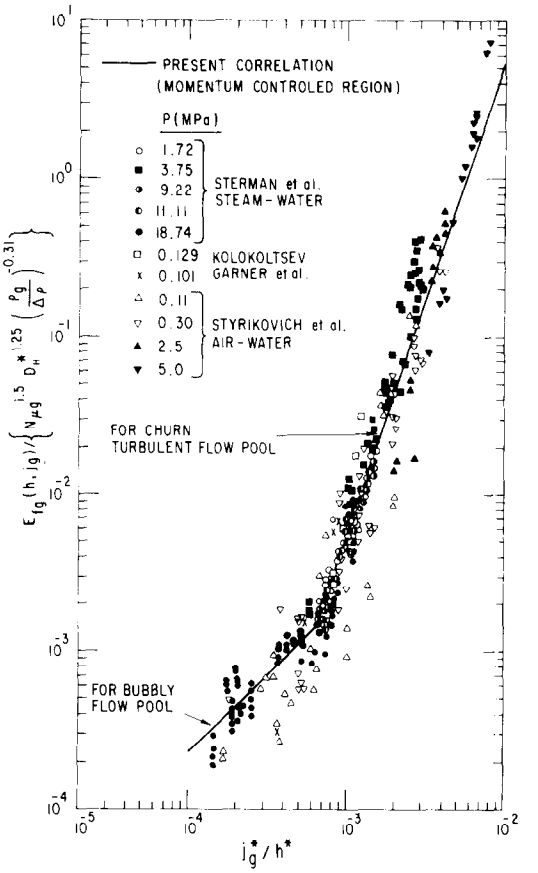

FIG. 9. Comparison of experimental data of various researchers [18, 21, 22, 23, 31] with predicted entrainment in the $E_{fg}/\{N_{\mu g}^{1.5} D_H^{*1.25} (\rho_g/\Delta\rho)^{-0.31}\}$ vs j_g^*/h^* plane.

change is caused by the flow regime transition in a liquid pool. As mentioned in Section 5, when the gas velocity is small, the flow regime becomes bubbly flow. The discrete bubbles rise up to the pool interface and collapse there. This is different from the mechanisms under which equation (52) is derived. In this bubbly flow regime, the droplet size distribution and initial velocity distribution may be quite different from those predicted by equations (21) and (37). This regime corresponds to the low gas flux regime previously mentioned. The change from the low to intermediate gas flux regime occurs approximately at j_g^* predicted by equation (23) which is derived from the criteria for the flow regime transition from bubbly to churn turbulent flow in a pool.

Although data are scarce and considerable scattering is observed, the entrainment in the low gas flux regime may be correlated by

$$E_{fg}(h,j_g) = 2.21 N_{\mu g}^{1.5} D_H^{*1.25} \left(\frac{\rho_g}{\Delta\rho}\right)^{-0.31} j_g^* h^{*-1}. \quad (53)$$

In Fig. 9, overall comparisons between the various experimental data and the above correlations are shown.

From equations (52) and (53) the transition criterion between the low and intermediate gas flux regimes can be obtained, thus

$$\frac{j_g^*}{h^*} = 6.39 \times 10^{-4}. \quad (54)$$

This criterion gives a higher value of j_g^* than that predicted by equation (23) over the range of h^* appeared in the experimental data. This is because in a boiling or bubbling pool system the void fraction is generally lower than those predicted by the standard drift flux model due to the significant internal circulation of liquid in the pool. Here h^* appears in the criterion due to the fact that the information at the interface to reach h^* requires a certain gas flux.

Figure 10 shows the various experimental data for entrainment in the

$$E_{fg} \text{ vs } (j_g^*/h^*)\, N_{\mu g}^{0.5} D_H^{*0.42} (\rho_g/\Delta\rho)^{-0.10}$$

plane. The solid line in this figure represents the correlation given by equation (52). This figure indicates that the correlation generally agrees well with the data, however, there is a systematic deviation at high values of j_g^*/h^*. This actually signifies the appearance of the high gas flux regime. This transition occurs

approximately at

$$\left(\frac{j_g^*}{h^*}\right) = 5.7\times10^{-4}N_{\mu g}^{-0.5}D_H^{*-0.42}\left(\frac{\rho_g}{\Delta\rho}\right)^{0.10} \quad (55)$$

or at

$$E_{fg} \simeq 1.0\times10^{-3}. \quad (56)$$

In the regime where (j_g^*/h^*) exceeds the value given by equation (55), the entrainment increases with (j_g^*/h^*) very rapidly as given by

$$E_{fg} \propto (j_g^*/h^*)^{7-20}. \quad (57)$$

The transition from the intermediate to high gas flux regime may be attributed to a flow regime transition in the liquid pool. The transition from churn-turbulent to annular, pseudo-jet or fountain flow [2, 51, 52] is indicated.

It may be possible to make a dimensionless correlation based on experimental data for this case. However, such a correlation is not very useful because it may give an unreasonably high value of entrainment at large j_g^* due to its high power dependence on j_g^*. Although no data are available, there should be an upper limit for entrainment in this regime. Here, as a first approximation, it is assumed that all the droplets produced at the pool surface are carried away. This limit is also predicted by the basic formulation given by equation (43) at $j_g^* \to \infty$ with the condition given by equation (48). Thus, the limit is obtained as

$$E_{fg}(h,j_g) \sim \lim_{j_g^*\to\infty}\int_0^{8.45j_g^{*-1}}\int_{v_{ti}^*}^{\infty}\delta(v_i^*-\bar{v}_i^*) \times 3.72\times10^{-4}\left(\frac{\rho_g}{\Delta\rho}\right)^{-1.0} j_g^{*1.5}D^{*0.5}\,dv_i^*\,dD^* = 2.48\times10^{-4}C_m^{1.5}j_g^{*1.5-3n_4/2}\left(\frac{\rho_g}{\Delta\rho}\right)^{-1.0}. \quad (58)$$

This value is identical to that in the near surface regime which is given by equation (49). Therefore, for practical purposes, the entrainment amount in the high gas flux might well be estimated by the correlation for the near surface region.

Now, based on the above analysis and correlation development, some of the underlining assumptions are reexamined. First, from equations (51) and (52), the proportionality constant in the correlation is now identified as

$$C = 74.77. \quad (59)$$

Furthermore, the coincidence of the exponents between equations (51) and (52) indicates that the assumption of the exponent of $\Delta\rho/\rho_g$ in the interface entrainment equation, equation (20), (in Section 4), can be justified.

9. ENTRAINMENT AMOUNT IN DEPOSITION CONTROLLED REGION

As shown in Section 7, beyond a certain height from the pool surface the entrainment consists only of the droplets having the terminal velocity less than the gas velocity. This phenomenon is also observed in some experiments [25, 26]. By neglecting the effect of the droplet deposition, the upper limit of the entrainment in this region can be expressed by equation (50).

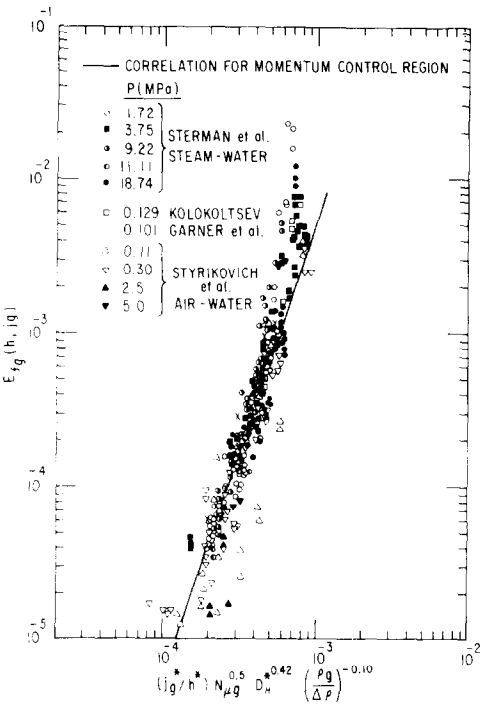

FIG. 10. Comparison of experimental data of various researchers [18, 21, 22, 23, 31] with predicted entrainment in the E_{fg} vs $(j_g^*/h^*)N_{\mu g}^{0.5}D_H^{*0.42}(\rho_g/\Delta\pi)^{-0.10}$ plane.

In an actual system, the entrainment amount decreases gradually with height h due to the deposition. The mass balance equation in the deposition controlled region is given by equation (60) assuming that there are no phase changes between liquid and gas, and no additional entrainment from the liquid film

$$\frac{dE_{fg}}{dh} = -\frac{4}{D_H}\frac{\dot{d}}{\rho_g j_g}. \quad (60)$$

Here $\dot{d}$ is the deposition rate of droplets (kg m^{-2} s^{-1}) and related to the mass concentration of droplets in the gas C_E(kg m^{-3}) by

$$\dot{d} = k_d C_E \quad (61)$$

where k_d is the droplet deposition coefficient (m s^{-1}) [2, 5]. When the velocity of droplets is approximately equal to the gas velocity, the droplet concentration C_E is given in terms of E_{fg} as

$$C_E = \rho_g E_{fg}. \quad (62)$$

Substituting equations (61) and (62) into equation (60) one obtains

$$\frac{dE_{fg}}{d(h/D_H)} = -4\left(\frac{k_d}{j_g}\right)E_{fg}. \quad (63)$$

Integration of equation (63) leads to an exponential

decay characteristic given by

$$E_{fg} \propto e^{-4(k_d/j_g)/(h/D_H)}. \quad (64)$$

In view of equations (50) and (64) experimental data of entrainment for the deposition controlled region [18, 26] are plotted in the $E_{fg}/\{j_g^{*3}N_{\mu g}^{0.5}(\rho_g/\Delta\rho)^{-1.0}\}$ vs h/D_H plane in Fig. 11. Although the data scatter considerably due to experimental uncertainties, they can be correlated by

$$E_{fg}(h,j_g) = 7.13\times10^{-4}j_g^{*3}N_{\mu g}^{0.5} \times\left(\frac{\rho_g}{\Delta\rho}\right)^{-1.0}\exp(-0.205(h/D_H)) \quad (65)$$

and $k_d = 0.051 j_g$.

The deposition coefficient calculated from equations (64) and (65) gives higher values of k_d than those observed in normal annular dispersed flow [53]. It is considered that droplets entrained from a bubbling or boiling pool have higher random velocity in the lateral direction when they are entrained. The deposition coefficient should increase due to this initial random momentum in the lateral direction. This situation is similar to the case where droplets are injected from a nozzle [50] into a pipe. In the latter case, the very high deposition rate near the injection nozzle is well known [2, 5, 54].

Comparing equations (52) and (65) the height above the pool surface at which the momentum controlled region changes to deposition controlled regime is given by

$$h^*\exp(-0.068(h^*/D_H^*)) = 1.97\times10^3 \times N_{\mu g}^{0.33}D_H^{*0.42}\left(\frac{\rho_g}{\Delta\rho}\right)^{0.23}. \quad (66)$$

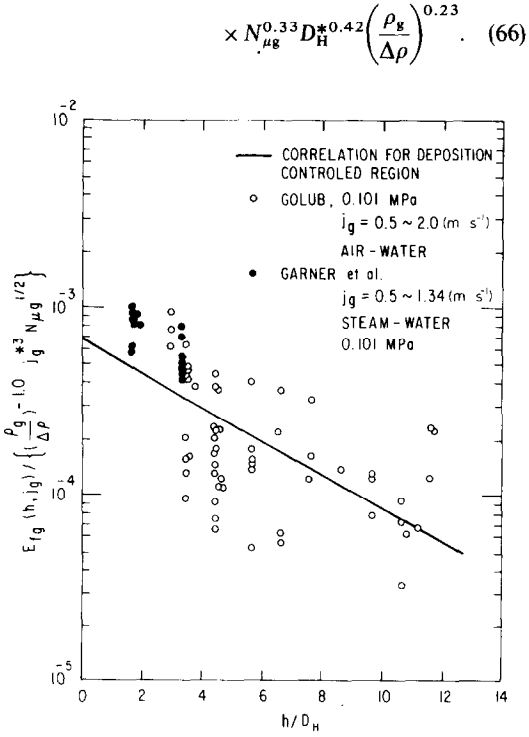

FIG. 11. Experimental data of entrainment in deposition controlled region [18, 26].

When the droplet deposition is small, equation (66) can be approximated by

$$h^* \simeq 1.97\times10^3 N_{\mu g}^{0.33}D_H^{*0.42}\left(\frac{\rho_g}{\Delta\rho}\right)^{0.23}. \quad (67)$$

10. ENTRAINMENT AMOUNT NEAR SURFACE REGION

In the near surface region, entrainment consists of all the entrained droplets from the pool surface. It is given by equation (49). Measuring the entrainment amount in this region is difficult because the pool surface is highly agitated. Therefore, the discrimination of entrained droplets from the agitated pool is quite difficult. The only data available in this near surface region are those of Rozen *et al.* [27, 28] who have obtained the data by extrapolating the measured entrainment in the momentum controlled region. The data are for an air–water system at atmospheric pressure. Their results show no dependence of E_{fg} on j_g and are given by

$$E_{fg} \simeq 4. \quad (68)$$

In view of equations (49) and (68), one obtains the correlation for the near surface region as

$$E_{fg}(h,j_g) = 4.84\times10^{-3}\left(\frac{\rho_g}{\Delta\rho}\right)^{-1.0}. \quad (69)$$

Equation (69) indicates that C_m and n_4 in equation (49) are given by

$$C_m = 7.24 \quad \text{and} \quad n_4 = 1. \quad (70)$$

From the above results, the maximum drop size correlation given by equation (49) can be rewritten as

$$D_{max}^* = 7.24 j_g^{*-1}. \quad (71)$$

Equation (71) implies that the maximum droplet size is fairly large, however, such large droplets only exist in the near surface region and their lifetime is considered to be very short.

From equations (52) and (69), the transition point between the near surface and momentum controlled regions is given by

$$h^* = 1.038\times10^3 j_g^* N_{\mu g}^{0.5}D_H^{*0.42}\left(\frac{\rho_g}{\Delta\rho}\right)^{0.23}. \quad (72)$$

Since equation (69) is obtained from a limited number of experimental data, further experimental works may be needed to verify the validity of the correlation given by equation (69) at high pressures.

11. SUMMARY AND CONCLUSIONS

Correlations for the droplet entrainment and carryover from a bubbling or boiling pool by streaming gas have been developed based on a simple mechanistic model of entrainment in collaboration with experimental data.

The analysis reveals that there are three regions of entrainment depending on the height above the pool

surface. For each region the correlation for the entrainment amount has been developed in terms of the dimensionless gas velocity j_g^*, height above surface h^*, gas viscosity number $N_{\mu g}$, vessel diameter D_H^*, and density ratio $(\rho_g/\Delta\rho)$. The results for the entrainment amount are summarized below.

11.1. *Near surface region* $(0 \leqslant h^* < h_2^*)$

This region is limited to the vicinity of the pool surface. In this region, entrainment consists of all droplets entrained at the pool surface and is given by equation (69).

11.2. *Momentum controlled region* $(h_2^* < h^* \leqslant h_1^*)$

This region is limited to the intermediate height range. The entrainment consists partly of the droplets which attain height h due to the initial momentum and partly of droplets whose terminal velocity is less than the gas velocity. This region is subdivided into three regimes, depending on the gas velocity:

(a) low gas flux regime, equation (53),
(b) intermediate gas flux regime, equation (52),
(c) high gas flux regime, equation (57).

11.3. *Deposition controlled region* $(h^* \geqslant h_1^*)$

In this regime, the deposition becomes the main factor determining the amount of entrainment. In this regime, the entrainment consists of droplets whose terminal velocity is less than the gas velocity. E_{fg} decreases gradually with h due to deposition and is given by equation (65).

11.4. *Entrainment rate and droplet size distribution*

From the above development for entrainment, it is now possible to obtain the entrainment rate and droplet size distribution at the pool surface. By integrating equation (21) over D with the limit given by equation (71), one gets

$$\frac{\dot{e}(j_g)}{\rho_g j_g}\int_0^\infty f(D,j_g)\,dD = 4.84\times10^{-3}\left(\frac{\rho_g}{\Delta\rho}\right)^{-1.0}. \quad (73)$$

In view of equation (10), the entrainment rate becomes

$$\dot{e}(j_g) = 4.84\times10^{-3}\rho_g j_g\left(\frac{\rho_g}{\Delta\rho}\right)^{-1.0}. \quad (74)$$

Thus the droplet size distribution becomes

$$f(D,j_g) = 0.077 j_g^{*1.5} D^{*0.5}\sqrt{\left(\frac{g\Delta\rho}{\sigma}\right)} \quad (75)$$

which applies to $D^* \leqslant D_{max}^*$ where $D_{max}^* = 7.27 j_g^{*-1}$.

11.5. *Total droplet flux*

In this work, the entrainment is correlated in terms of the upward droplet flux j_{fe}. This parameter itself is very important in studying the carryover droplet mass. However, it is noted that the total liquid volumetric flux j_f may be different from the upward droplet flux j_{fe} due to the droplets and liquid film which are falling back to the pool. For quasi-steady-state conditions, it is straightforward to extend the present analysis to obtain the total liquid flux as discussed below.

For simplicity, the effect of the deposition is neglected. In this case, it can easily be shown from the continuity relation that the total liquid flux can be given by the droplet flux at the end of the momentum controlled region, thus from equation (50)

$$\frac{\rho_f j_f}{\rho_g j_g} = 2.0\times10^{-3} j_g^{*3} N_{\mu g}^{0.5}\left(\frac{\rho_g}{\Delta\rho}\right)^{-1.0}. \quad (76)$$

This is because all the droplets arriving at the end of the momentum controlled region are fully suspended and cannot fall back without deposition. Then the droplet volumetric flux of the falling drops are given by

$$j_{fd} = j_f - j_{fe} \quad (77)$$

which is generally negative in the near surface or momentum controlled regions. This indicates that there are a definite number of droplets falling downward in these regions.

The comparison of the above entrainment correlations with a large number of data showed good agreement over a wide range of pressure. This indicates that the present mechanistic model is accurate. Furthermore, it explains the basic physical processes of pool entrainment and the existence of the different regions and regimes of entrainment. Therefore, the present results supply valuable information which has not been available previously.

Acknowledgements—The authors would like to express their appreciation to Drs N. Zuber, Y. Y. Hsu, and M. Young of NRC for valuable discussions on the subject. This work was performed under the auspices of the U.S. Nuclear Regulatory Commission.

REFERENCES

1. M. Ishii and M. A. Grolmes, Inception criteria for droplet entrainment in two-phase cocurrent film flow, *A.I.Ch.E.* **21**, 308 (1975).
2. G. F. Hewitt and N. S. Hall-Taylor, *Annular Two-phase Flow*. Pergamon Press, Oxford (1970).
3. M. Ishii and K. Mishima, Liquid transfer and entrainment correlation for droplet-annular flow, *Proc. 7th Int. Heat Transfer Conf.*, TF 20, Munich (1982).
4. I. Kataoka, M. Ishii and K. Mishima, Generation and size distribution of droplet in annular two-phase flow, *Trans. Am. Soc. Mech. Engrs, J. Fluid Engn* **105**, 230 (1983).
5. I. Kataoka and M. Ishii, Mechanism and correlation of droplet entrainment and deposition in annular two-phase flow, ANL-82-44, NUREG/CR-2885 (1982).
6. R. S. Brodkey, *The Phenomena of Fluid Motion*. Addison-Wesley, Reading, Massachusetts (1967).
7. M. Ishii, *Thermo-fluid Dynamic Theory of Two-phase Flow*. Eyrolles, Paris, Scientific and Medical Publication of France, New York (1975).
8. A. J. Shor, H. T. Ward, D. Miller and W. A. Rodger, Radioactive carry-over from Borax-III and test systems, *Nucl. Sci. Engn* **2**, 126–142 (1957).
9. B. Manowitz, R. H. Bretton and R. V. Horrigan, Entrainment in evaporators, *Chem. Engng Prog.* **51**(7), 313 (1955).
10. N. Mitsuishi, S. Sakata, Y. Matsuda and Y. Yamamoto, The liquid entrainment and its removal of large scale

evaporation unit—evaporation of radioactive liquid waste, *J. Atom. Energy Soc. Japan* **1**(6), 363 (1959).
11. H. J. Viecenz and F. Mayinger, Comparison of phase separation models by use of own experimental data, *Proc. NATO Adv. Study Inst. on Two-phase Flow and Heat Transfer*, 1983, Istanbuhl (1976).
12. H. M. Lee and G. E. McCarthy, Liquid carry-over in air–water countercurrent flooding, *Proc. 7th Int. Heat Transfer Conf.*, TF-7, Munich (1982).
13. T. Iguchi, Carryover from a liquid pool with vertical air flow, *Trans. Jap. Chem. Engng. Soc.* **8**(3), 225 (1982).
14. S. I. Cheng and A. J. Teller, Free entrainment behavior in sieve trays, *A.I.Ch.E.* **7**(2), 283 (1961).
15. F. A. Zenz and N. A. Weil, A theoretical–empirical approach to the mechanism of particle entrainment from fluidized beds, *A.I.Ch.E. Jl* **4**(4), 473 (1958).
16. R. H. Perry and C. H. Chilton, *Chemical Engineers Handbook* (5th edn). McGraw-Hill, New York (1973).
17. G. C. K. Yeh and N. Zuber, On the problem of liquid entrainment, ANL-6244 (1960).
18. F. H. Garner, S. R. M. Ellis and J. A. Lacey, The size distribution and entrainment of droplets, *Trans. Instn. Chem. Engrs* **32,** 222 (1954).
19. G. N. Kruzhilin, The dependence of the permissible vapor load upon the pressure, *Izv. Akad. Nauk. Otd. Tekh. Nauk.* No. 7, 1106 (1951).
20. M. A. Styrikovich, L. S. Sterman and A. V. Surnov, An investigation of carry over of salt by using radioactive isotopes, *Teploenergetika* **2**(2), 43 (1955).
21. L. S. Sterman, A. I. Antonov and A. V. Surnov, An investigation of steam quality at 185 atm, *Teploenergetika* **4**(3), 17 (1957).
22. L. S. Sterman, On the theory of steam separation, *J. Tech. Phys.* **28**(7), 1562 (1958).
23. M. A. Styrikovich, V. I. Petukhov and V. A. Kolokoltsev, The effect of gas phases density on the extent of droplet entrainment, *Teploenergetika* **11**(11), (1964).
24. V. I. Petukhov and V. A. Kolokoltsev, Effect of liquid viscosity on droplet entrainment and volumetric air content, *Teploenergetika* **12**(9), 30 (1965).
25. A. M. Rozen, S. I. Golub, I. F. Davydov and G. I. Gostinin, Some law governing drop carry over, *Sov. Phys.-Dokl.* **14**(7), 648 (1970).
26. S. I. Golub, Investigation of moisture carryover and separation in evaporation apparatus, Candidates Dissertation, MEI (1970) (quoted from ref. [46]).
27. A. M. Rozen, S. I. Golub and I. F. Davydov, Entrainment of moisture at small distance from a bubbling surface, *Sov. Phys.-Dokl.* **19**(6), 338 (1974).
28. A. M. Rozen, S. I. Golub and T. I. Votintseva, Calculating droplet carryover with bubbling, *Teploenergetika* **23**(11), 59 (1976).
29. A. M. Rozen, S. I. Golub and T. I. Votintseva, On the nature of degree of dependence of transported carryover on vapor velocity with bubbling, *Teploenergetika* **23**(9), 55 (1976).
30. A. M. Rozen, G. I. Gostinin, I. F. Davydov, S. I. Golub and A. N. Krasikov, On the problem of effects of salt content in water on moisture carryover with bubbling, *Izv. Akad. Nauk. Energetika Transp.* No. 6, 164 (1973).
31. V. A. Kolokoltsev, Investigation of the operation of the steam space of ISV evaporator, Trudy MEI (1952) (quoted from ref. [40]).
32. M. Ishii and N. Zuber, Drag coefficient and relative velocity in bubbly, droplet or particulate flows, *A.I.Ch.E. Jl* **25,** 843 (1979).
33. I. Kataoka and M. Ishii, Mechanistic modeling and correlations for pool entrainment phenomenon, Argonne National Laboratory Report, ANL-83-37, NUREG/CR-3304 (1983).
34. R. F. Davis, The physical aspect of steam generation at high pressure and problem of steam contamination, *Proc. Inst. Mech. Engrs* **144,** 198 (1940).
35. D. M. Newitt, N. Dombrowski and F. M. Knelman, Liquid entrainment, 1. The mechanism of drop formation from gas or vapor bubble, *Trans. Inst. Chem. Engrs* **32,** 245 (1954).
36. V. G. Gleim, On the problem for general theory on moisture entrainment from boiling mixture, *Zhu. Prikl. Khimii* **28**(1), 12 (1955).
37. V. G. Gleim, I. K. Shelomov and B. R. Shidlovskii, Process leading to generation of droplets in rupture of bubbles at liquid–gas interface, *J. Appl. Chem. USSR* **32**(1), 222 (1959).
38. S. Aiba and T. Yamada, Studies on entrainment, *A.I.Ch.E. Jl* **5**(4), 506 (1959).
39. G. B. Wallis, *One Dimensional Two-phase Flow*, pp. 261–263. McGraw-Hill, New York (1969).
40. M. Ishii, One-dimensional drift-flux model and constitutive equations for relative motion between phases in various flow regimes, ANL-77-47 (1977).
41. M. Ishii and K. Mishima, Study of two-fluid model and interfacial area, ANL-80-111, NUREG/CR-1873 (1980).
42. R. D. Nielsen, M. R. Tek and J. L. York, Mechanism of entrainment formation in distillation columns, University of Michigan, Ann Arbor, Michigan (1966).
43. L. S. Akselrod and G. M. Yusova, Dispersity of the liquid in the interplate space in bubble tower, *J. Appl. Chem. USSR* **30,** 739 (1959).
44. R. L. Muller and R. G. H. Prince, Regimes of bubbling and jetting from submerged orifices, *Chem. Engng Sci.* **27,** 1583 (1972).
45. T. H. Margulova, An experimental investigation of the relative velocity of vapor in bubbling through a layer of water at high pressures, *Trans. Power Inst., M. V. Molotov,* **11,** (1953) (quoted from ref. [33]).
46. A. V. Kurbatov, The bubbling and the problem of critical load in steam separation, *Trans. Power Inst., M. V. Molotov,* **11,** (1953) (quoted from ref. [33]).
47. L. S. Sterman, The generalization of experimental data concerning the bubbling of vapor through liquid, *Sov. Phys.–Tech. Phys.* 1479 (1957).
48. J. F. Wilson, R. J. Grenda and J. F. Patterson, Steam volume fraction in a bubbling two-phase mixture, *Trans. ANS* **5** Ser. 151 (1962).
49. C. E. Lapple and C. B. Shepherd, Calculation of particle trajectory, *Ind. Engng Chem.* **32**(5), 605 (1940).
50. J. O. Hinze, Fundamentals of the hydrodynamic mechanism of splitting in disperson process, *A.I.Ch.E. Jl* **1,** 289 (1955).
51. N. Zuber and J. A. Findley, Average volumetric concentration in two-phase flow systems, *Trans. Am. Soc. Mech. Engrs*, Series C, *J. Heat Transfer* **87,** 453 (1965).
52. K. W. Orth, M. Epstein, J. H. Linehan, G. A. Lambert and L. J. Stachyra, Hydrodynamic aspects of volume boiling, ANL/RAS 80-6 (1980).
53. I. I. Paleev and B. S. Filipovich, Phenomena of liquid transfer in two-phase dispersed annular flow, *Int. J. Heat Mass Transfer* **9,** 1089 (1966).
54. L. E. Gill and G. F. Hewitt, Sampling probe studies of the gas core in annular two-phase flow—Part 3. Distribution of velocity and droplet flowrate after injection through axial jet, AERE-M1202 (1967).

MODELISATION MECANISTE ET FORMULATION POUR LE PHENOMENE D'ENTRAINEMENT EN RESERVOIR

Résumé—L'entrainement d'un liquide par l'ébullition en réservoir est très important en pratique dans l'évaluation de sûreté des réacteurs nucléaires dans les cas transitoires hors norme ou dans les accidents tels que la perte de réfrigérant et la chute de débit accidentelles. Des gouttelettes qui quittent la surface libre sont en partie enlevées par un courant gazeux et en partie renvoyées sur la surface libre par gravité. On développe une formule pour l'évaluation de l'entrainement basée sur un modèle simple mécaniste et sur un certain nombre de données. Cette analyse révèle qu'il existe trois régions d'entrainement dans la direction axiale depuis la surface libre. Dans la première région (près de la surface) l'entrainement est indépendant de la hauteur et de la vitesse du gaz. Dans la seconde région (contrôlée par la quantité de mouvement) le débit d'entrainement décroît quand la hauteur augmente et croît avec la vitesse du gaz. Dans la troisième région (région contrôlée par le dépôt), l'entrainement croît avec la vitesse du gaz et diminue quand la hauteur augmente à cause du dépôt des gouttelettes. La formulation s'accorde bien avec un grand nombre de données expérimentales, dans un large domaine de pression pour des systèmes air–eau et vapeur d'eau–eau liquide.

EIN MECHANISTISCHES MODELL UND KORRELATIONEN FÜR BEHÄLTER-ENTRAINMENT-PHÄNOMENE

Zusammenfassung—Entrainment aus einem Flüssigkeitsbehälter (beim Sieden oder Sprudeln) ist von beachtlicher praktischer Bedeutung für Sicherheits-Berechnungen von Kernreaktoren unter abnormalen Übergangszuständen oder Unfällen wie Kühlmittelverlust oder Strömungsstillstand. Tropfen, die von einer freien Oberfläche suspendieren, werden teilweise durch ein strömendes Gas abtransportiert und kehren teilweise durch die Schwerkraft zur freien Oberfläche zurück. Für die Entrainmentmenge im Behälter wurde eine Korrelation entwickelt, die auf einem einfachen mechanistischen Modell und einer Anzahl von Daten basiert. Diese Untersuchung verdeutlicht, daß drei Bereiche des Entrainment in axialer Richtung oberhalb der Flüssigkeitsoberfläche existieren. Im ersten Bereich (nahe der Flüssigkeitsoberfläche) ist des Entrainment unabhängig von der Höhe und der Gasgeschwindigkeit. Im zweiten Bereich (impulskontrollierter Bereich) sinkt die Entrainmentmenge mit zunehmendem Abstand von der freien Oberfläche und erhöht sich mit steigender Gasgeschwindigkeit. Im dritten Bereich (durch Abscheidung kontrollierter Bereich) steigt das Entrainment mit steigender Gasgeschwindigkeit an und nimmt mit zunehmender Höhe entsprechend der Tropfenabscheidung ab. Die vorliegende Korrelation stimmt gut mit einer großen Anzahl von experimentellen Daten über einen weiten Druckbereich für Luft–Wasser- und Dampf–Wasser-Systeme überein.

МЕХАНИСТИЧЕСКОЕ МОДЕЛИРОВАНИЕ И ОБОБЩЕННОЕ ОПИСАНИЕ ЯВЛЕНИЯ УНОСА В БОЛЬШОМ ОБЬЕМЕ ЖИДКОСТИ

Аннотация—Исследование уноса из большого объема жидкости при кипении или барботаже имеет большое практическое значение для оценки безопасности ядерного реактора при отклонении от стационарного режима работы или авариях с утечкой теплоносителя или тепла. Капли, находящиеся во взвешенном состоянии над свободной поверхностью, частично уносятся потоком газа, а частично возвращаются на свободную поверхность под действием силы тяжести. На основе простого механистического моделирования и ряда экспериментальных данных предложено соотношение для определения количества уносимого вещества. Анализ показывает, что можно выделить три области уноса в осевом направлении от поверхности жидкости. В первой области (у поверхности) унос не зависит от расстояния от поверхности и скорости газа. Во второй (определяемой переносом импульса) количество уносимой жидкости уменьшается с увеличением скорости газа. В третьей (контролируемой осаждением капель) унос увеличивается с ростом скорости газа и уменьшается с увеличением расстояния от поверхности из-за осаждения капель. Полученное соотношение хорошо согласуется с большим числом экспериментальных данных в широком диапазоне изменения давления для систем воздух–вода и пар–вода.